International Journal of Modelling and Simulation

ISSN: (Print) (Online) Journal homepage: https://www.tandfonline.com/loi/tjms20

Performance investigation on ANFIS and FFNN assisted direct and indirect PV-fed switched reluctance motor water pumping system

Vijay Babu Koreboina, Narasimharaju B L & Vinod Kumar D M

To cite this article: Vijay Babu Koreboina, Narasimharaju B L & Vinod Kumar D M (2021): Performance investigation on ANFIS and FFNN assisted direct and indirect PV-fed switched reluctance motor water pumping system, International Journal of Modelling and Simulation, DOI: 10.1080/02286203.2021.1875288

To link to this article: https://doi.org/10.1080/02286203.2021.1875288

Published online: 27 Jan 2021.

INTERNATIONAL JOURNAL OF MODELLING AND SIMULATION
https://doi.org/10.1080/02286203.2021.1875288

Taylor & Francis
Taylor & Francis Group

ARTICLE

Performance investigation on ANFIS and FFNN assisted direct and indirect PV-fed switched reluctance motor water pumping system

Vijay Babu Koreboina [a], Narasimharaju B L [b] and Vinod Kumar D M [b]

[a]Department of Mechatronics Engineering, Manipal Institute of Technology, Manipal Academy of Higher Education, Manipal, Karnataka, India; [b]Department of Electrical Engineering, National Institute of Technology Warangal, Warangal, Telangana, India

ABSTRACT

Alternative energy sources have impacted as the ideal choice for reducing the burden on the grid and producing clean energy for water pumping. As an alternative to conventional motors for pumping, switched reluctance motor (SRM) is promising, cost-effective and highly efficient. This paper presents artificial intelligence (AI) supported variable voltage angle control (VVAC) for indirect and direct photovoltaic (PV)-fed SRM-based water pumping systems (WPS). Proposed feedforward neural network (FFNN) and adaptive neuro-fuzzy inference system (ANFIS) models are simulated and analysed for their percentage average error and real-time execution speed in the dSPACE-1104 control board. ANFIS resulted in $1/10^{th}$ reduction of execution time and improved performance accuracy in contrast to FFNN counterparts. A 4kW, 8/6 SRM model, has been developed in MATLAB/Simulink environment to validate the proposed system for both direct and indirect schemes. Further, the performance comparison of peak current, RMS current, torque ripple, and efficiency for direct and indirect PV-fed systems are presented in this work. These comparative assertions reveal the feasibility of both the methods with good performance. Moreover, a reduction in overall system size and cost with the absence of an intermediate converter, the direct method provides a reduced torque ripple as compared to the indirect counterpart.

ARTICLE HISTORY
Received 12 July 2020
Accepted 9 January 2021

KEYWORDS
Artificial Nero-Fuzzy Inference (ANFIS); dSPACE Real-Time Controller; feedforward Neural Network (FFNN); photovoltaic (PV) Pump; switched Reluctance Motor (SRM)

1. Introduction

Water resources play a major role in various sectors like agriculture, domestic needs, etc. Likewise, economic growth mainly depends on the agriculture sector. Most of the off-grid rural areas need portable alternative clean energy to drive the water pumps. Extending the grid to those remote areas would be capital-intensive and also inefficient due to transmission and distribution losses. In addition, carbon emission and thermal fuel extinction call for clean alternative energy sources (AES) such as biomass, solar, wind, and hybrid. At present, these resources contribute to electricity generation by about 19% [1]. Therefore, small-scale AES are an ideal choice to reduce the burden on the grid, and to produce clean energy for water pumping systems. In the present scenario, conventional electrical motors (induction motors, synchronous motors, permanent magnet synchronous motors, and permanent magnet DC motors) are employed for PV-fed water pumping and household power generation. Switched reluctance motor (SRM) is an alternative candidate which is promising, cost-effective, and highly efficient in contrast to the conventional motors for small-scale applications. With its wider advantages, SRM has emerged in research importance for variable speed drive applications. With the absence of carbon brushes, slip rings, commutators, and cage bars, SRM has emerged in its suitability for wide applications such as hand fork, train air conditioner, and aerospace [2].

Conventional control of SRM with fixed DC-bus voltage requires chopping operation at lower speeds and single pulse angle control at higher speeds. Chopping control has limitations of switching loss and noise, which can be overcome by using variable DC-bus voltage angle control in contrast to the conventional counterpart [3,4]. A few authors in the literature [5–13] have addressed SRM for standalone PV-fed WPS application. Table 1 provides an overview of the state of the art on PV-fed SRM-WPS application. As perceived from the literature overview, many of the control schemes proposed for PV-fed SRM-WPS generally require sensors, an intermediate DC-DC converter stage, and a power conditioning unit. Thus, with a brief review of these control strategies for PV-fed SRM water pumping systems, the paper proposes a variable voltage angle control (VVAC) of direct and

CONTACT Vijay Babu Koreboina vijaybabukoreboina@gmail.com Department of Mechatronics Engineering, Manipal Institute of Technology, Manipal Academy of Higher Education, Manipal, Karnataka, 576 104, India.

Table 1. Overview of the state of the art on PV-fed SRM-WPS application.

Authors	SRM objective	SRM Control Scheme	Key features
Deepak, 2012 [5]	Torque ripple minimization	DTC HCM with solar radiation and temperature effect	Reduced DC link voltage
Sweta B, 2012 [6]	Direct coupled PV SRM pump	HCM with solar radiation effect	Modelling and simulation Elimination of the converter stage
Hamid M, 1998 [7]	Performance Analysis of PV pump using SRM	SPM with solar radiation effect	Improvement in matching efficiency
Oshaba, 2015 [8]	PI design for MPPT	- - - -	Advantages of BAT algorithm compared with PSO
Oshaba, 2015 [9]	PV-fed speed control of SRM	- - - -	Ant colony optimization compared with GA
Sujitha, 2014 [10]	Standalone PV-fed SRM using Repression Resistor Converter	Conventional Low-speed hysteresis and high-speed angle pulse	Energy stored in the dump resistor to improve torque production
Oshaba, 2013 [11]	High-speed SRM fed by PV	SPM	A torque and speed control loops for accurate speed control
Dursun, 2008 [12]	Fuzzy logic speed control for PV-fed SRM drive	- - - -	Intelligent speed control to improve destination distance of the wheelchair
Bhim Singh, 2016 [13]	SPV-fed SRM pump using intermediate cuk converter	SPM for speed using varying DC link	Reduce ringing effect and reduce losses in the intermediate converter stage

indirect PV-fed pumping systems. Further, with the ability to process knowledge under ever-changing situations, artificial intelligence (AI) techniques (like NN, FUZZY, ANFIS, genetic algorithms (GA)) have been increasingly used in the control of power converters, electric drives, and power systems [14–16]. This paper presents two methods of AI techniques; feedforward neural network (FFNN) and adaptive neuro-fuzzy inference system (ANFIS) assisted VVAC for PV-fed SRM system. The performance parameters such as phase peak current, RMS current, torque ripple and efficiency play a major role for SRM to evaluate its suitability in various applications. Hence, these parameters are to be investigated in specific with FFNN and ANFIS assisted direct and in-direct PV-fed SRM water pumping system.

Section-II presents the VVAC strategy for the proposed system with an introduction from section-I. Section-III presents the implementation of FFNN and ANFIS-based VVAC. Finally, Section-IV presents simulation, result analysis, and performance comparisons of various parameters of the proposed system.

2. VVAC for PV-fed SRM-based water pumping system

Switched reluctance machine is gaining importance in rural off-grid applications. Authors [17] have presented a state-of-the-art review on control strategies and suitability of SRM for off-grid applications such as PV water pumping system, wind energy conversion system, and hybrid PV-wind system. A brief review of the PV-fed SRM water pumping system shows a wider scope in its applications. A direct torque-controlled (DTC) SRM drive is reported [5]. DTC controlled drive shows the merit of reduction in torque ripple. However, it also needs the hysteresis band and current sensors to implement. The modelling and simulation of hysteresis torque-controlled SRM water pumping systems is proposed and discussed [6]. Performance analysis of PV pumping systems using SRM drive is studied [2]. Matching efficiency between PV array and the proposed system is found to be around 95% with operating efficiency as 85% during most of its operating time.

SRM conventional control strategy with fixed DC-bus voltage requires chopping control at low speeds and angle control at higher speeds. In the lower speed chopping control range, control parameters are I_{ref}^{*}, T_{on} and T_{off} angles. At a higher speed angle control range, the only two parameters T_{on} and T_{off} angles would suffice to meet the required torque demand. Chopping control has the limitations of higher switching losses, noise, sensor requirement, and frequency limiter. Authors [3,4] suggested speed-dependent variable DC-bus voltage to overcome the limitations of chopping control at lower speeds and to operate only in angle control mode throughout the speed range.

VVAC strategy is addressed for indirect-coupled linear speed-voltage variation and direct-coupled nonlinear speed-voltage variation of the proposed system. For the indirect system, linear speed-voltage variation is realized using a DC chopper, as shown in Figure 1(A). Chopper output is regulated in-line with the reference speed from the maximum power point of the PV system. With an angle control mode, required torque levels at different speeds can be achieved by varying T_{on} and T_{off} angles [4,18]. To simplify the VVAC strategy further, T_{off} can be fixed and T_{on} is varied to achieve various speed-torque levels. With the step increments of speed and torque, the T_{on} angle for various speed-torque levels is estimated by extensive simulation iterations. Figure 1(A) shows the block diagram of an indirect PV-fed SRM system with a linear speed-voltage

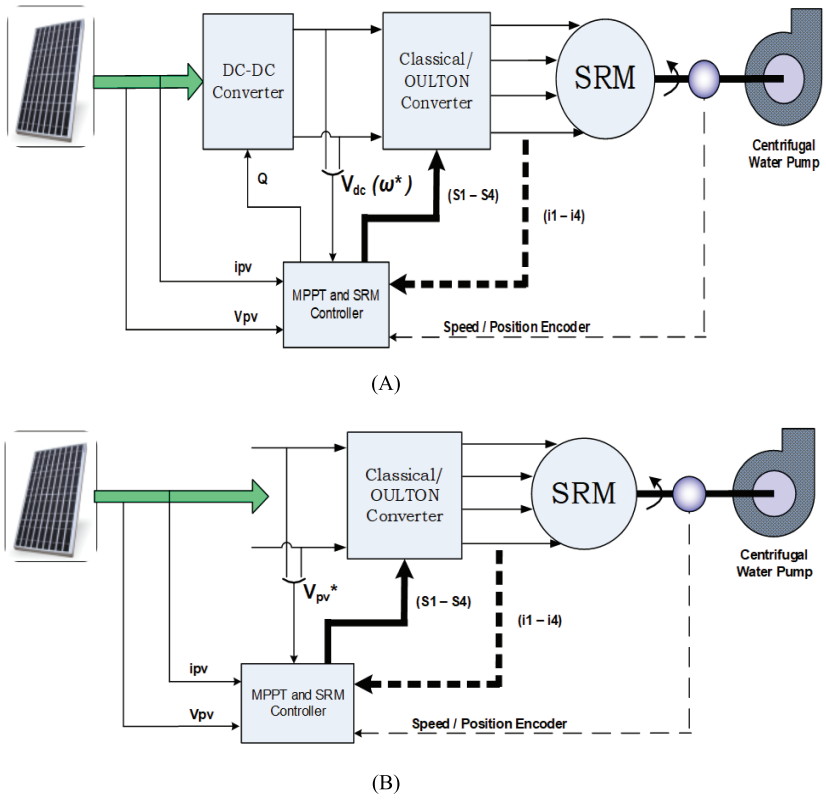

Figure 1. (A)Indirect coupled with linear speed-voltage control. (B) Direct-coupled non-linear speed-voltage control.

control scheme. Figure 1(B) illustrates the block diagram of a direct PV-fed SRM system with a non-linear speed-voltage control scheme.

The PV array used in the study consists of 10 parallel strings, 748 cells in series per string, such that the overall terminal voltage v_{array} and P_{array} at ambient temperature are given by (1) and (2) [19]. Figures 2(A) and 2(B) show the volt-current and power-voltage characteristics of the PV model at various insolation levels, respectively. A 4 kW 8/6 SRM model [3,4] is used for the simulation study, and its flux-linkage and static torque characteristics are shown in Figures 3(A) and 3 (B). Based on (3) and (4) centrifugal pump load is modelled. Figure 4(A) to 4(C) illustrates pump torque-speed (load) characteristics, Insolation versus P_{max}, curves and insolation versus speed (ω) at P_{max}, respectively. With the use of operating points, SRM is operated in angle control mode for different speeds varying T_{on} to

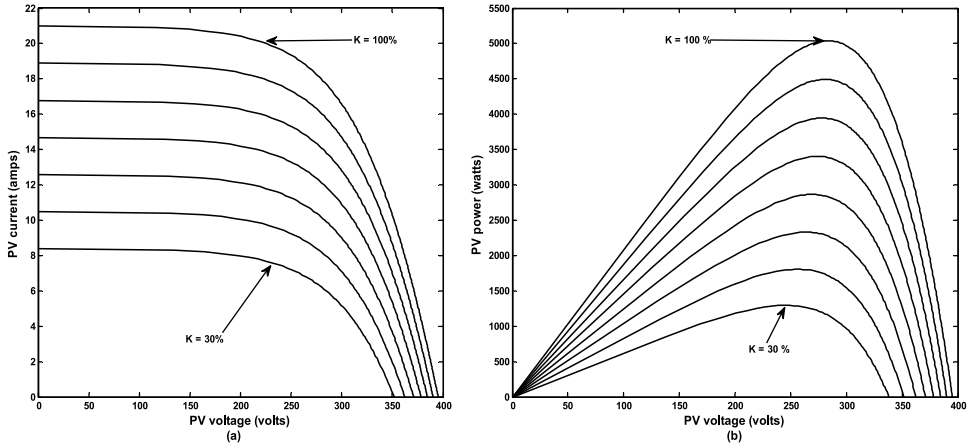

Figure 2. PV characteristics for different insolation values (k), (A) Current-voltage, (B) Power-voltage.

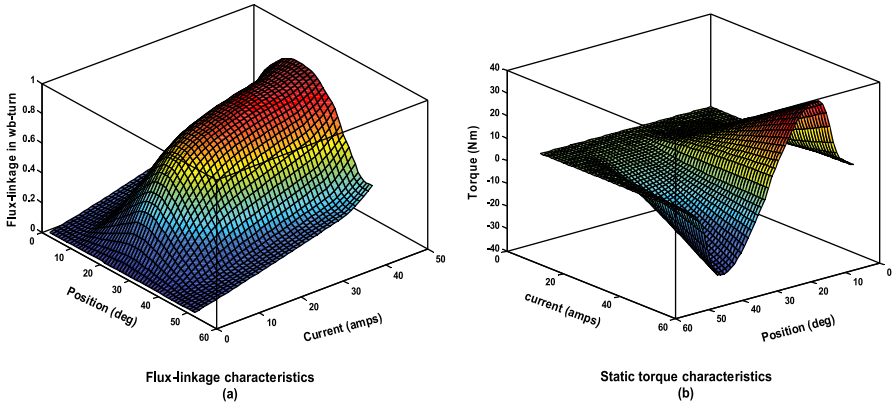

(A) 3D flux-linkage characteristics, (B) 3D Static-Torque characteristics.

Figure 3. (A) 3D flux-linkage characteristics,(B) 3D Static-Torque characteristics.

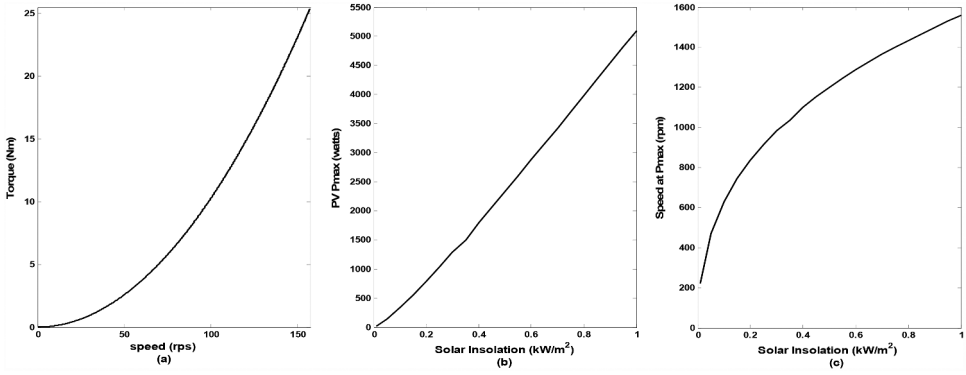

Figure 4. (A) Pump torque-speed (load) characteristics, (B) Insolation vs P_{max}, (C) Insolation vs ω at P_{max}.

achieve the required torque levels. Figures 5(A) and 5(B) show the speed–voltage relationship and T_{on} angles required in fixed T_{off} to achieve different torque levels at different speeds for indirect PV-fed system. Figures 5

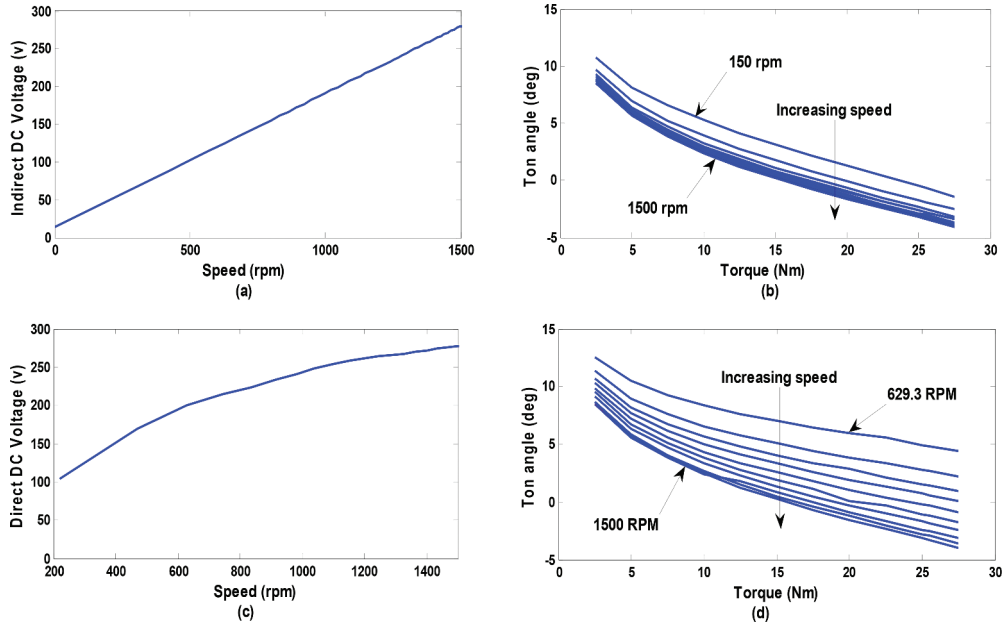

Figure 5. (A) Linear speed-voltage relationship, (B) Torque vs T_{on} for different speed levels with indirect. (C) Non-linear speed-voltage relationship, (D) Torque vs T_{on} for different speed with for direct.

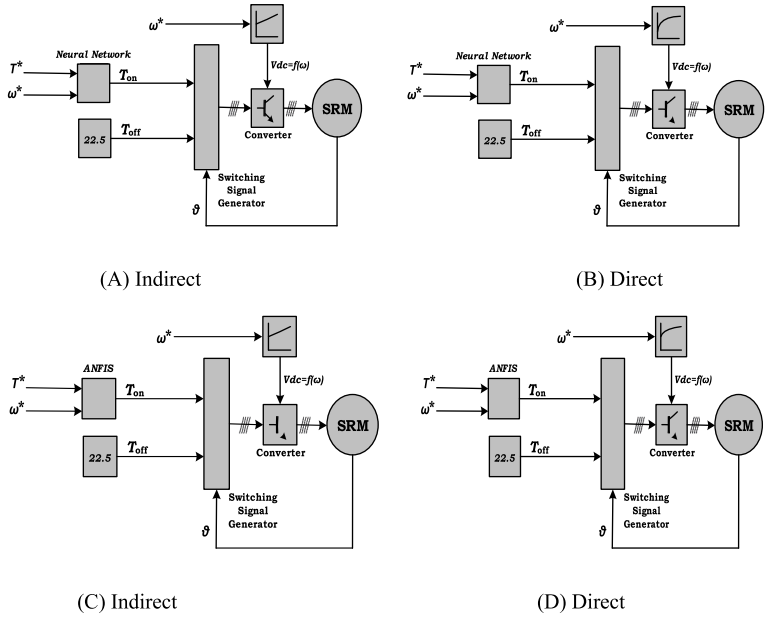

Figure 6. Block diagram of NN and ANFIS based Direct & Indirect Methods for SRM PV Water Pump (A) Indirect, (B) Direct, (C) Indirect, (D) Direct.

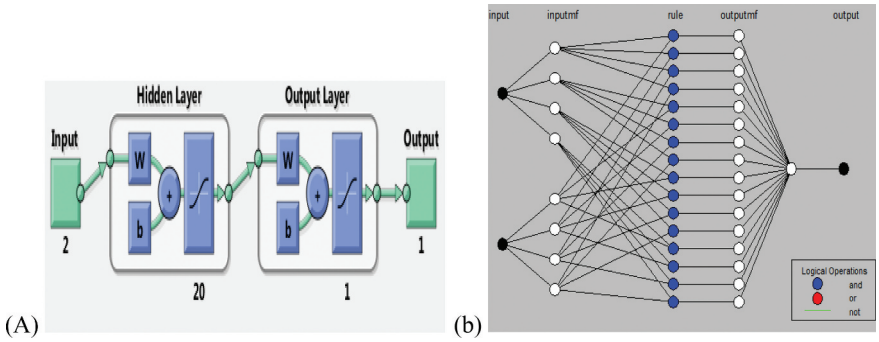

Figure 7. MATLAB models for angle control using (A) FFNN, (B) ANFIS.

Table 2. Simulated T_{on} angle for different speed and torque levels for the indirect-coupled system.

w T	150 rpm	350 rpm	450 rpm	600 rpm	750 rpm	900 rpm	1050 rpm	1200 rpm	1350 rpm	1500 rpm
2.5 Nm	10.79	9.72	9.28	9.05	8.95	8.8	8.7	8.67	8.56	8.55
5 Nm	8.17	6.95	6.4	6.18	6.1	5.9	5.83	5.75	5.65	5.64
7.5 Nm	6.53	5.22	4.66	4.38	4.29	4.1	4.03	3.95	3.81	3.8
10 Nm	5.25	3.88	3.29	3	2.9	2.7	2.62	2.55	2.41	2.4
12.5 Nm	4.13	2.75	2.14	1.85	1.76	1.55	1.45	1.38	1.23	1.21
15 Nm	3.15	1.74	1.1	0.84	0.75	0.52	0.43	0.37	0.19	0.19
17.5 Nm	2.21	0.81	0.2	−0.09	−0.175	−0.4	−0.49	−0.57	−0.73	−0.75
20 Nm	1.29	−0.07	−0.69	−0.97	−1.04	−1.27	−1.37	−1.41	−1.59	−1.62
22.5 Nm	0.40	−0.91	−1.53	−1.79	−1.852	−2.08	−2.18	−2.24	−2.42	−2.43
25 Nm	−0.5	−1.75	−2.36	−2.61	−2.625	−2.87	−2.96	−3.04	−3.21	−3.22
25.5 Nm	−0.67	−1.89	−2.49	−2.76	−2.78	−3.03	−3.13	−3.19	−3.39	−3.39
27.5 Nm	−1.42	−2.55	−3.17	−3.4	−3.41	−3.7	−3.77	−3.84	−4.04	−4.04

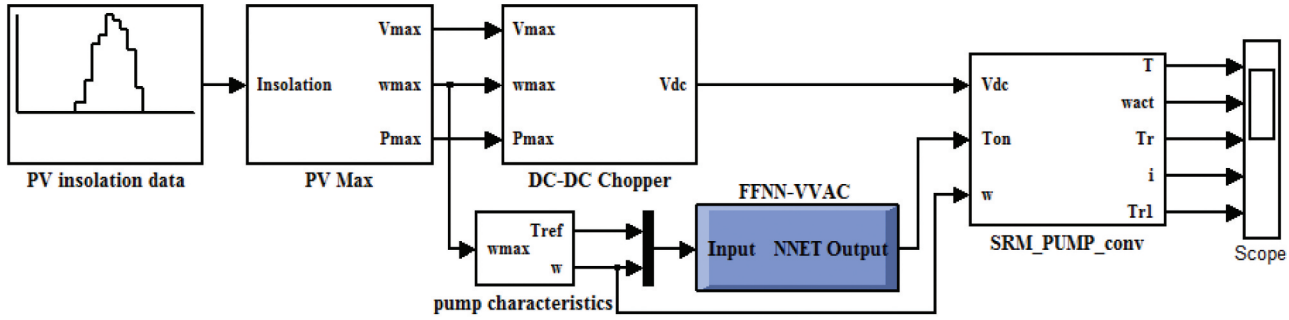

(a) FFNN VVAC Indirect PV-fed SRM system model

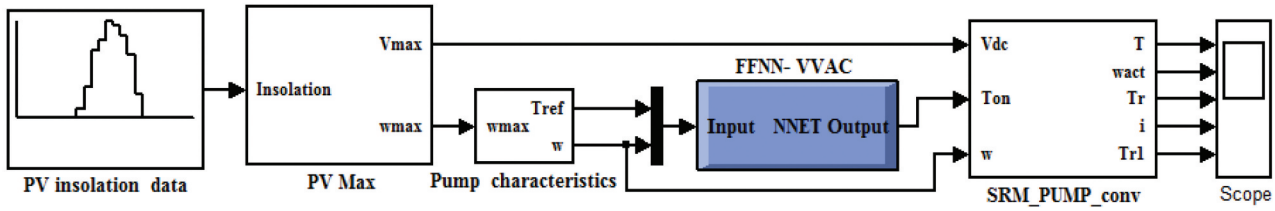

(b) FFNN VVAC Direct PV-fed SRM system model

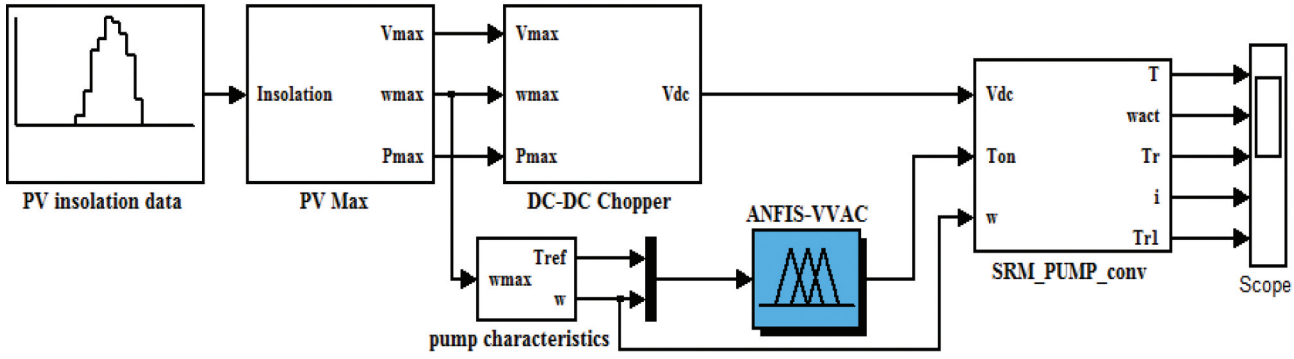

(c) ANFIS VVAC Indirect PV-fed SRM system model

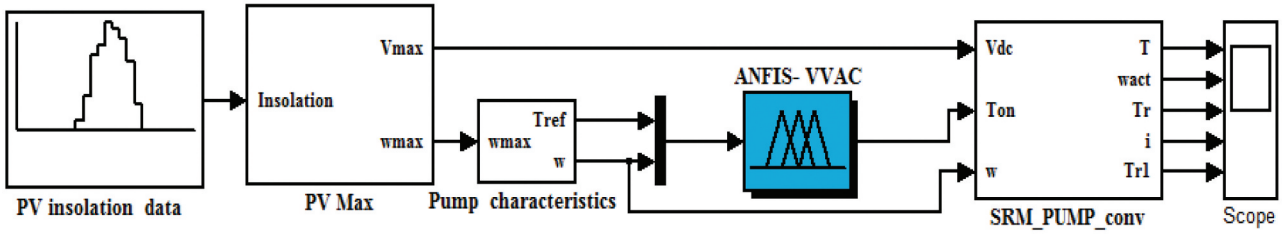

(d) ANFIS VVAC Direct PV-fed SRM system model

Figure 8. Simulation models of indirect and direct PV-fed proposed system.

Table 3. Simulated T_{on} angle for different speed and torque levels for the direct-coupled system.

w T	629.3 rpm	831.4 rpm	974.6 rpm	1089 rpm	1186 Rpm	1270 rpm	1346 rpm	1414 rpm	1476 rpm	1500 rpm
2.5 Nm	12.58	11.35	10.7	10.3	9.8	9.5	9.18	8.5	8.65	8.48
5 Nm	10.47	8.98	8.23	7.71	7.18	6.75	6.38	5.6	5.85	5.63
7.5 Nm	9.23	7.58	6.74	6.17	5.55	5.1	4.67	3.8	4.01	3.8
10 Nm	8.34	6.56	5.65	5.03	4.37	3.83	3.39	2.42	2.66	2.42
12.5 Nm	7.65	5.75	4.78	4.11	3.38	2.8	2.3	1.81	1.5	1.23
15 Nm	7.04	5.06	4.01	3.31	2.54	1.91	1.37	0.84	0.5	0.24
17.5 Nm	6.49	4.45	3.36	2.6	1.78	1.1	0.5	−0.05	−0.39	−0.7
20 Nm	5.96	3.87	2.86	1.93	1.07	0.03	−0.27	−0.86	−1.23	−1.55
22.5 Nm	5.55	3.32	2.14	1.31	0.4	−0.35	−1	−1.64	−2.04	−2.37
25 Nm	4.93	2.78	1.56	0.71	−0.24	−1.04	−1.71	−2.4	−2.8	−3.15
25.5 Nm	4.82	2.67	1.45	0.57	−0.36	−1.16	−1.86	−2.54	−2.97	−3.32
27.5 Nm	4.41	2.21	0.96	0.1	−0.89	−1.72	−2.43	−3.15	−3.6	−3.98

(C) and 5(D) show the speed–voltage relationship and T_{on} angles also required for its fixed T_{off} to achieve different torque levels at various speeds for direct PV-fed system. The relevant equations of PV are,

$$v_{array} = 47.3688 * \log_{\ell}\left(\frac{I_{ph} - I_{array} + 0.005}{0.005}\right) - 1.296 * I_{array} \quad (1)$$

$$p_{array} = 47.3688 * \log_{\ell}\left(\frac{I_{ph} - I_{array} + 0.005}{0.005}\right)^{2} - 1.296 * I^{2}_{array} \quad (2)$$

where I_{array} is the array current, I_{ph} is the insolation dependent photocurrent.

$$T_L = 0.00103 * \omega^2 \quad (3)$$

$$P_L = 0.00103 * \omega^3 \quad (4)$$

At PV maximum point,

$$P_L = \eta * P_{\max} = 0.00103 * \omega^3 \quad (5)$$

$$\omega^3 = \sqrt[3]{\frac{\eta * P_{\max}}{0.00103}} \quad (6)$$

3. FFNN and ANFIS based VVAC strategy for SRM

FFNN is a biologically inspired method of a parallel distributed processor with its natural property to store experimental knowledge. An ANFIS incorporates the advantages of both FFNN and fuzzy logic, which provides a fuzzy modelling procedure to compute output with a learning method similar to a neural network. In general, neural networks, fuzzy, and ANFIS are used in SRM for position sensorless control, where nonlinearity in flux-linkage characteristics is used to compute rotor position [20–22]. With the use of AI techniques, modelling of flux-linkage and torque ripple minimization in SRM applications is reported [23–27]. Very few authors have worked on AI techniques in PV-fed SRM pumping systems to study MPPT techniques [28,29]. FFNN and ANFIS techniques are known for their higher parallel computational and easy adaptive capabilities. In this way, FFNN and ANFIS assisted VVAC methods are simulated and analysed for both indirect and direct PV-fed system to compute T_{on} angle for required torque and speed level. Figure 6(A) and 6(B) depict FFNN assisted VVAC for direct and indirect PV-fed systems, respectively. Accordingly, Figures 6(C) and 6(D) illustrate ANFIS assisted VVAC for direct and indirect PV-fed systems, respectively. Selection is made between FFNN and ANFIS assisted VVAC, which is based on the percentage average error [27] and the performance of real-time execution [21].

3.1. Realization of FFNN assisted VVAC

The main agenda of the multilayer FFNN network model is to compute T_{on} angle for various speed and

Table 4. Percentage average error of FFNN and ANFIS.

Data samples Model	121 Indirect coupled	121 Direct coupled	1614 Indirect coupled	1614 Direct coupled
NN5	14.32	4.70	2.40	0.81
NN10	2.34	2.79	1.09	0.58
NN15	3.02	2.03	0.97	0.57
NN20	1.60	2.81	0.92	**0.53**
ANF9	17.71	3.58	9.03	1.02
ANF16	11.06	2.73	3.89	0.97
ANF25	6.16	2.06	1.72	0.77
ANF36	4.36	1.93	1.44	**0.57**

Table 5. dSPACE execution time of FFNN and ANFIS.

Data samples	121		1614	
Model	Indirect coupled	Direct coupled	Indirect coupled	Direct coupled
NN5	76.1us	75.57us	75.32us	75.28us
NN10	83.8us	83.4us	83.71us	83.63us
NN15	88.072us	89.32us	89.35us	89.23us
NN20	94.17us	93.6us	92.02us	**93.6us**
ANF9	4.9us	4.5us	5us	5.21us
ANF16	5.89us	5.4us	6.17us	6.13us
ANF25	9.1us	8.8us	9.2us	9.8us
ANF36	9.9us	9.4us	10.2us	**10.9us**

torque levels. The network consists of three layers, i.e., input, hidden, and output layers. It is set with a 'sigmoidal' activation function for the hidden layer and the 'linear' activation function for the output layer. The input layer has two input neurons and one at the output, where the system is tested for 20, 15, 10, and 5 neurons in the hidden layer. Despite this, larger neurons in the hidden layer lead to the overfit and effects for realization. The network is trained with a supervised Levenberg-Marquardt backpropagation algorithm with data sets given in Tables 1 and 2 for

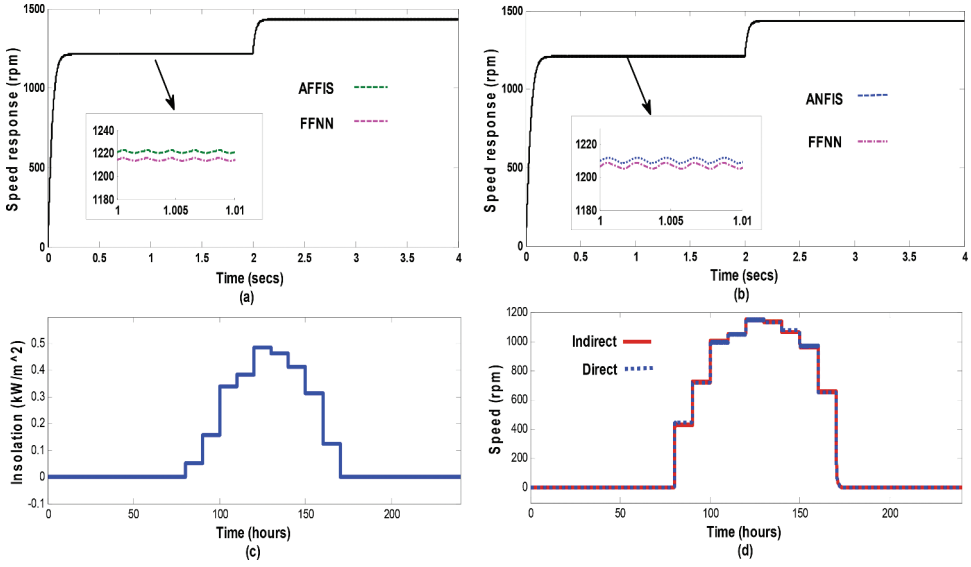

Figure 9. Speed response: (A) & (B) FFNN and ANFIS assisted VVAC with step change of insolation (0.55 to 0.85) (C) Insolation of a day in summer, (D) Speed response for insolation of a day in summer.

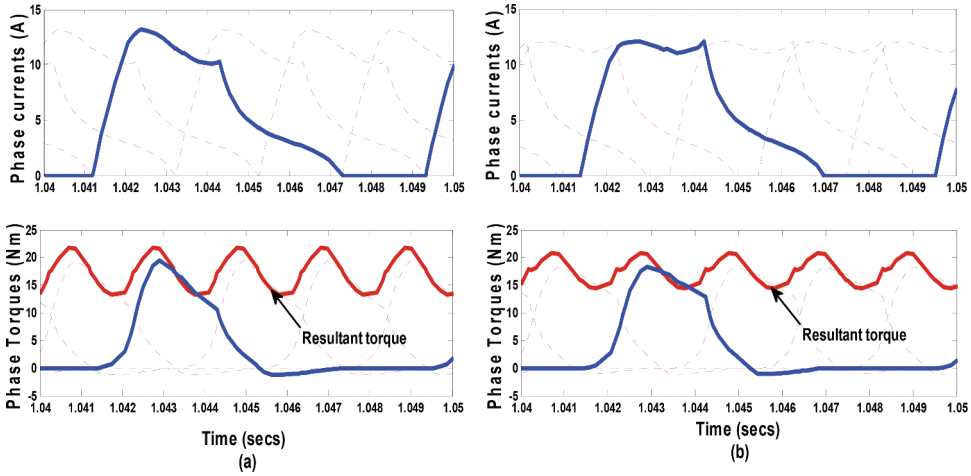

Figure 10. Phase currents, phase and resultant torque with 0.55 insolation. (A) Indirect coupled system and (B) Direct-coupled system.

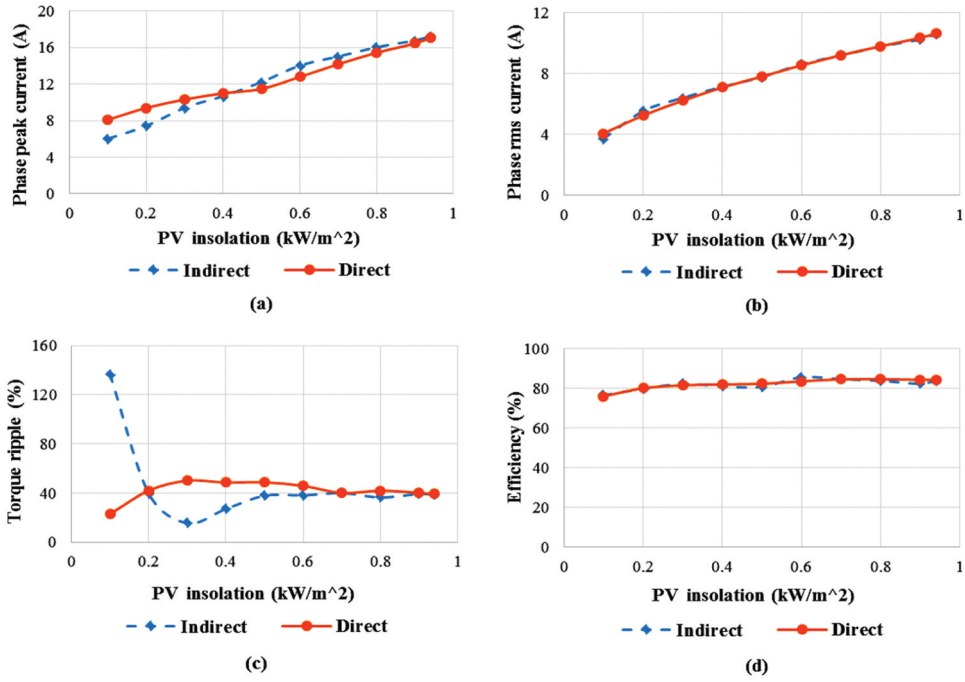

Figure 11. Performance characteristics of indirect coupled and direct-coupled system in terms of. (A)Phase peak current, (B) Phase RMS current, (C) Torque ripple, (D) Efficiency.

the indirect and direct methods, respectively. The weights are randomly generated from small positive and negative values to ensure that the network is unsaturated. In this way, four FFNN network models are trained (2–20-1, 2–15-1, 2–10-1 and 2-5-1) and tested for the T_{on} angle estimation. Steps involved in FFNN model realization are as follows:

1.Network topologies are generated with 20, 15, 10 and 5 neurons. Here Figure 7(A) shows the network structure to compute T_{on} angle in MATLAB/Simulink.

2.Supervised learning is employed to train the network with input data sets of speed and torque, and the output T_{on} angle.

3.Testing and validation of the network in terms of percentage average error from the actual T_{on} of simulated data with the FFNN T_{on} output.

4.Testing of real-time execution

3.2. Realization of ANFIS assisted VVAC

ANFIS incorporates the advantages of the adaptive nature of the neural network and associates a fuzzy inference system to track the input–output relationship. ANFIS has the ability to represent the rules proposed by Takagi and Sugeno. This constructs a membership function based on the nature of data by using the

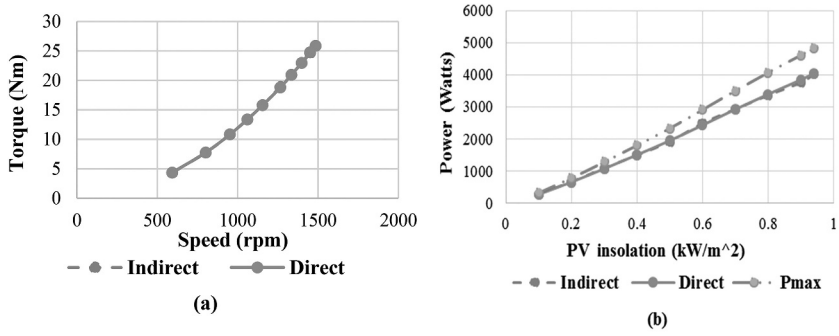

Figure 12. Performance characteristics of indirect coupled and direct-coupled system in terms of. (A) Output torque-speed characteristics, (B) Output power.

learning method, which in turn works similar to that of a neural network. Here, the triangular membership function is used with the backpropagation algorithm to train the network. Steps involved in ANFIS model realization are as follows:

1.Data from the simulation is loaded into the ANFIS editor. It is arranged in terms of column vectors, where the last column vector represents output T_{on} and the remaining column vectors are treated as inputs.

2.Generating the FIS structure based on fuzzy rules and the membership functions for both inputs is as shown in Figure 7(B).

3.To generate the membership functions, the FIS network is trained by using a backpropagation algorithm.

4.Simulated data is compared with the model output-data validation in terms of percentage average error.

5.Testing of real-time execution

3.3. Comparative analysis of FFNN and ANFIS assisted VVAC

The proposed FFNN and ANFIS VVAC models evaluated and compared with simulated data from Tables 2 and 3 for both indirect and direct systems, respectively. The performance comparative analysis has been made in terms of percentage average error and real-time execution. For the error analysis of FFNN and ANFIS models, the percentage average error is presented as in equation (7). From this analysis, a percentage average error is obtained for each of the models. Table 4 describes the percentage average error of FFNN (with 5, 10, 15, and 20 neurons) and ANFIS (with 9, 16, 25, and 36 rules) for indirect and direct systems. From Table 4, the analysis shows that FFNN models are giving less error compared to the ANFIS model. Besides, it can be observed from Table 3, that FFNN models with neurons of 20, 15 and 10 provide better performance in contrast with 5 neuron counterparts. Further, from Table 4, it is evident that models with 121 samples of the indirect and direct system results in larger percentage errors which are usually unacceptable. Therefore, to improve the accuracy of the models, sample data are pre-expanded up to 1614 using linear interpolation. When the models are trained with the expanded samples, it is observed that there is sufficient and significant improvement in ANFIS accuracy and found to be the same as FFNN shown in Table 4.

$$\%ge\ Average\ Error\ = \frac{\sum \ell}{\sum T_{on}} * 100 \tag{7}$$

where Σe- summation of all error samples in the T_{on} computed from models with respect to simulated data. ΣT_{on}- summation of all samples computed T_{on} angles.

Although the models developed resulted in significantly improved accuracy with increased samples, the performance of real-time execution analysis is considered to be an important aspect. Therefore, the models are tested for real-time execution by using dSPACE 1104 turnaround time. For FFNN and ANFIS, the off-line trained networks experimented individually, and the results are tabulated for both indirect and direct control methods as given in Table 5. It is observed in Table 5 that the FFNN is taking more execution time compared to the ANFIS in both indirect and direct methods. Table 4 also indicates that for higher data samples of 1614, ANFIS provides a 1/10th reduction in execution time and improved performance accuracy in contrast to FFNN counterparts. Thus, VVAC is realized using FFNN and ANFIS to study the response in both indirect and direct systems.

4. Simulation and results analysis of proposed system

MATLAB/Simulink simulation models of indirect and direct PV-fed systems developed with FFNN, ANFIS VVAC schemes are depicted in Figure 8. DC-DC converter with switching frequency of 25 kHz, inductor (L) = 2 mH, capacitor (C) = 26 μF designed for indirect PV-fed system to get varied DC voltage [18,19]. Figures 9(A) and 9(B) reveal that the speed response of SRM for a step-change in insolation from 0.55 to 0.85 kW/m^2 in both indirect and direct schemes using FFNN and ANFIS VVAC. It can be observed from Figures 9(A) and 9(B) that both result in good response and justify their application for PV-fed SRM-based water pumping system. Figure 9(C) shows the one-day solar insolation data in summer at NIT, Warangal collected from National Renewable Energy Laboratory (NREL), USA. Figure 9(D) illustrates the speed response of both indirect and direct scheme with the use of VVAC for one-day solar insolation that is shown in Figure 9(C). It is being observed from Figure 9(D) that both indirect and direct systems are giving better responses for change in insolation levels over one-day period. Figure 10 illustrates phase currents, phase torques, and resultant torque at 0.55 kW/m^2 insolation.

The performance comparison of various system parameters likewise; peak current, RMS current, torque ripple, efficiency, output speed-torque characteristics and output power at different insolation levels as shown in Figure 11. It can be observed from Figure 11 (A), that the peak current of both indirect and direct methods is well within limits of rated value of 18 A, which can make ensure the safe operating conditions of the proposed system. The RMS current represents the I^2R loss component of SRM. From Figure 11(B), it is observed that the RMS current of both indirect and direct methods are closer to the same levels at all insolation. Torque ripple is a measure of smooth response and noise levels of SRM. Minimization of torque ripple results in an improved speed response and reduced noise levels. It can be observed from the Figure 11(C) that except at very lower insolation levels, torque ripple in the direct system is less as compared to the indirect system. Further, Figure 11(D) shows the efficiency of both methods is near to the same as for all insolation levels. To understand SRM performance in pumping application using indirect and direct schemes, SRM output torque-speed characteristics are illustrated in Figure 12(A) and it shows that both methods are matching the pump load performance characteristics. Figure 12(B) shows the output power for both the methods where it can be observed that both methods are giving the same output power at various insolation levels.

These comparisons confirm that at nearly the same peak current, RMS current, power and efficiency, direct coupled system results in reduced torque ripples. In addition to these, with the near same performance and reduced torque ripple, VVAC direct PV-fed system operates without an intermediate stage, current feedback sensors and frequency limiters.

5. Conclusion

Switched reluctance machine has been gaining valuable importance for variable speed drive applications due to its several advantages: simple and rugged construction, high efficiency, high torque to inertia ratio and thermal robustness. This paper presents VVAC for direct and indirect PV-fed SRM water pumping system using FFNN and ANFIS techniques. FFNN and ANFIS models are simulated and then percentage average error is estimated. Also, those execution times are compared using the dSPACE-1104 real-time control board. FFNN results in a lesser percentage average error with higher execution time in contrary to ANFIS counterpart. ANFIS resulted in $1/10^{th}$ reduction of execution time and improved performance accuracy in contrast to FFNN counterparts. The result analysis reveals that the AI-assisted VVAC gives good transient and steady-state speed response for both direct and indirect systems.

Performance comparison of direct and indirect coupled systems in terms of phase peak current, phase RMS current, torque ripple, efficiency, output torque-speed characteristics and output power are presented. A 4 kW OULTON 8/6 SRM is used to study these control strategies for the proposed system. With this, it is observed that for near the same peak current, RMS current, power, and efficiency, a direct PV-fed system resulted in a reduced torque ripple. The proposed VVAC for PV-fed SRM water pumping systems resulted in the following advantages:

- Simplified control scheme.
- No requirement for current sensors and limiters as in HCM.
- Does not require of intermediate DC-DC converter thus simplifies the control scheme and facilitates the direct PV-fed variable speed drives.
- Contrary to the indirect method, the direct method also eliminates the intermediate converter and provides a reduced torque ripple at lower insolation levels.
- ANFIS based VVAC results in a $1/10^{th}$ reduction of execution time and improved performance accuracy in comparison to FFNN.

Aforesaid assertions reveal that the proposed ANFIS assisted VVAC control scheme with a direct PV-fed SRM water pumping system provides better performance with reduced converter stage.

Acknowledgement

This research work is supported under the Scheme for IMPacting Research INnovation and Technology (IMPRINT) project funded by MHRD, Government of India with file no IMP/2019/000295.

Disclosure statement

No potential conflict of interest was reported by the authors.

Notes on contributors

Dr. Vijay Babu Koreboina pursued his Bachelor degree in Electrical and Electronics Engineering from B. V. B College of Engineering and Technology, Hubli, Karnataka in the year 2008. He has completed his Masters of Technology in Power Electronics from B. M. S. College of Engineering, Bangalore in 2012. He has several publications in reputed Journals and Conferences at National and International levels. He is currently working as Assistant Professor at Department of

Mechatronics, Manipal Institute of Technology, Manipal Academy of Higher Education, Manipal, Karnataka, India.

Dr. Narasimharaju B. L was born in Gowribidhanur, Karnataka, India on May 20, 1975. He received B.E and M.E degree in Electrical Engineering, from University Visveswaraya College of Engineering, Bangalore University, India in 1999 and 2002 respectively. He obtained his PhD degree from Indian Institute of Technology Roorkee, in 2012. His areas of interests in Bidirectional converter, Power Electronic Drives and LED lighting systems. He has several publications in reputed Journals and Conferences at National and International levels. He is currently working as Faculty in Electrical Engineering, National Institute of Technology Warangal, India.

Prof. D. M. Vinod Kumar obtained his B.E. (Electrical) and M.Tech. (Power Systems) degrees from Osmania University, Hyderabad, during 1979 and 1981 respectively. He obtained his Ph.D. Degree from IIT Kanpur in the year 1996. The title of his thesis is "Artificial Neural Network based Power System State Estimation". During 2002-03 he was Post Doctoral Fellow at Howard University, Washington DC, USA. He has published more than 70 papers in International Journals and conferences. His areas of interest are Power systems Operation and Control, Power System Stability and Security, AI techniques for Power System and Renewable Energy Systems. At present he is Professor of Electrical Engineering at National Institute of Technology, Warangal.

ORCID

Vijay Babu Koreboina http://orcid.org/0000-0002-9994-548X

References

[1] Singh D, Sharma NK, Y R S, et al. Global status of renewable energy and market: Future prospectus and target. Int. Conf. on sustainable energy and intelligent systems, SEISCON 2011, Chennai, India. p. 171–176.
[2] Krishnan R. Switched reluctance motor drives modeling, Simulation, Analyses, Design, and applications. London: CRC Press; 2001.
[3] Debiprasad Panda RV. Reduced acoustic noise variable DC-Bus-Voltage-Based sensorless switched reluctance motor drive for HVAC applications. IEEE Trans Industrial Electron. 2007;54(4):2065–2078.
[4] Koreboina VB, Venkatesha L. Modelling and simulation of switched reluctance generator control for variable speed wind energy conversion systems. Int. Conf. IEEE Power Electronics Drives and Energy Systems Conference, PEDES 2012, Bangalore. p. 1–6.
[5] Ronanki D, Parthiban P PV-Battery powered direct torque controlled switched reluctance motor drive. Proc. Int. Conf. Power and Energy Engineering Conference, Shanghai; 2012. p. 1–4.
[6] Sweta B, Chakravarti A, Raju AB. Mathematical modelling and simulation of directly coupled PV water pumping system employing switched reluctance motor. Int. Conf. IEEE PES Innovative Smart Grid Technologies, India; 2011. p. 386–390.
[7] Hamid MBM, Anis WR. Performance analysis of PV pumping systems using switched reluctance motor drives. Elsevier J Solar Energy. 1996;56(2):161–168.
[8] Oshaba AS, Ali ES, Abd Elazim SM. PI controller design for MPPT of photovoltaic system supplying SRM via BAT search algorithm. Neural Comput Appl. 2017;28(4):651–667.
[9] Oshaba AS, Ali ES, Abd Elazim SM. ACO based speed control of SRM fed by photovoltaic system. Int J Electric Power Energy Syst. 2015;67:529–536.
[10] Sujitha S, Venkatesh C. Analysis of regulated PV fed switched reluctance motor drives using repression resistor converter. Int J Eng Technol. 2014;6(3):1309–1313.
[11] Oshaba AS. Control strategy for a high speed SRM fed from a photovoltaic source. Res J Appl Sci Eng Technol. 2013;6(17):3174–3180.
[12] Dursun M. A wheelchair driven with fuzzy logic controlled switched reluctance motor supplied by PV arrays. J Appl Sci. 2008;8(19):3351–3360.
[13] Singh B, Mishra AK, Kumar R. Solar powered water pumping system employing switched reluctance motor drive. IEEE Trans Industrial Appl. 2016;52(5):3949–3957.
[14] Langer N, Bhat AH, Agarwal P. Neural-network-based space-vector pulse-width modulation for capacitor voltage balancing of three-phase three-level improved power quality converter. IET Power Electron. 2014;7(4):973–983.
[15] Narasimharaju BL, Dubey SP, Singh SP. Performance evaluation of fuzzy logic controlled bidirectional DC to DC converter. Int J Computing Sci Commun Technol. 2011;3(2):598–603.
[16] Vinod Kumar DM, Srivastava SC, Shah S, et al. Topology processing and static state estimation using artificial neural networks. IEE Generation, Transmission Distribution. 1996;143(1):99–105.
[17] Koreboina VB, Narasimharaju BL, Vinod Kumar DM. Switched reluctance machine for off-grid rural applications: A review. T&F IETE Techn Rev. 2016;33(4):428–440.
[18] Xu R YZ, Zhong L, Chen A, et al. Analytical method to optimise turn-on angle and turnoff angle for switched reluctance motor drives. IET Electr Power Appl. 2012;6(9):593–603.
[19] Nabil. M, Allam SM, Rashad EM. Modeling and design considerations of a photovoltaic energy source feeding a synchronous reluctance motor suitable for pumping systems. Ain Shams Engg J. 2012;3(4):375–382.
[20] Zhong R, Wang YB, Xu YZ. Position sensorless control of switched reluctance motors based on improved neural network. IET Electr Power Appl. 2012;6(2):111–121.
[21] Paramasivam S, Vijayan S, Vasudevan M, et al. Verification of AI based rotor position estimation techniques for a 6/4 pole switched reluctance motor drive. IEEE Trans Magnetics. 2007;43(7):3209–3222.
[22] Mese E, Torrey DA. An approach for sensorless position estimation for switched reluctance motors using artificial neural networks. IEEE Trans Power Electron. 2002;17(1):66–75.
[23] Bay OF, Elmas C. Modeling of the inductance variation and control of the switched reluctance motor based on

fuzzy logic. T&F Intelligent Automation Soft Computing. 2013;10(3):233–246.

[24] Song S, Lefei G, Ma S, et al. Accurate measurement and detailed evaluation of static electromagnetic characteristics of switched reluctance machines. IEEE Trans Instrum Meas. 2015;64(3):704–714.

[25] Chai JY, Liaw CM. Reduction of speed ripple and vibration for switched reluctance motor drive via intelligent current profiling. IET Electr Power Appl. 2010;4 (5):380–396.

[26] Shang C, Reay D, Adapting WB. CMAC neural networks with constrained LMS algorithm for efficient torque ripple reduction in switched reluctance motors. IEEE Trans Control Syst Technol. 1999;7(4):401–413.

[27] Lachman T, Mohamad TR, Fong CH. Nonlinear modelling of switched reluctance motors using artificial intelligence techniques. IEE Electric Power Appl. 2004;151(1):53–60.

[28] Ali ES. Speed control of DC series motor supplied by photovoltaic system via firefly algorithm. Neural Comput Appl. 2015;26:1321–1332.

[29] Oshaba AS, Ali ES, Abd Elazim SM. Speed control of SRM supplied by photovoltaic system via ant colony optimization algorithm. Neural Comput Appl. 2015;28:365–374.